Measurement of the double-differential neutron cross section of UO_2 from room temperature to hot full power conditions

Gilles Noguere[1,*], *Shuqi* Xu[1], *Alain* Filhol[2], *Jacques* Ollivier[2], *Emmanuel* Farhi[2], and *Yoan* Calzavara[2]

[1]CEA,DEN Cadarache, Saint Paul Les Durance, France
[2]Institut Laue Langevin, Grenoble, France

Abstract. Experimental phonon densities of states of UO_2 have been deduced from double-differential neutron scattering data measured at 300 K, 600 K and 900 K using the IN6 time-of-flight spectrometer of the Institute Laue-langevin (ILL). The comparison with *ab intio* phonon spectra obtained at the North Caroline South University from first-principle calculations confirms that harmonic vibrations of the atoms cannot accurately reproduce the phonon broadening related to the oxygen atoms.

1 Introduction

The slow-neutron scattering properties of uranium dioxide (UO_2) has been the subject of many experimental and theoretical studies since the pioneer works reported in the sixties [1, 2]. Major results about the acoustic and optical vibration modes of UO_2 were published in a series of symposia on neutron scattering and neutron thermalization organized by the International Atomic Energy Agency, between 1960 and 1977 [3, 4]. At room temperature, crystal dynamics properties of UO_2 have been well described by Dolling using dispersion curves measured at the triple-axis-crystal spectrometer at Chalk River [5]. Despite major experimental and theoretical improvements, Pang [6, 7] recently shows that first-principles phonon density of states (PDOS) simulations cannot accurately reproduce inelastic neutron scattering measurements for UO_2, carried out at 295 K and 1200 K using the ARCS spectrometer of the Spallation Neutron Source (SNS). Large differences between experiments and calculations are attributed to an anharmonic linewidth broadening, which is observable even at room temperature. The present work aims to complement the work of Pang by providing experimental phonon densities of states for UO_2 from room temperature to 900 K in order to stimulate theoretical studies for improving comparison to experiment.

2 Governing equations

In the low neutron energy range, typically below 1 eV, the slowing down of neutrons in UO_2 is affected by the chemical bonds between the uranium and oxygen atoms. The incoherent scattering approximation allows to neglect the interference terms and to express the double differential scattering cross section of each atom separately. If T is the temperature of the target and k_B is the Boltzmann constant, the temperature-dependent double differential scattering cross section for $X = {}^{238}$U (or $X = {}^{16}$O) in UO_2 can be written as [8]:

$$\frac{d^2\sigma^T_{n_X}}{dE'd\theta} = \frac{\sigma^0_{n_X}}{2k_BT}\sqrt{\frac{E'}{E}}\,\mathrm{e}^{-\beta/2}S^T_X(\alpha,\beta), \tag{1}$$

where $\sigma^0_{n_X}$ is the neutron scattering cross section at $T = 0$ and $S^T_X(\alpha,\beta)$ is the symmetric form of the so-called thermal scattering law [9], which is defined as a function of the momentum transfer q:

$$\alpha = \frac{q^2\hbar^2}{2M_Xk_BT} = \frac{E' + E - 2\mu\sqrt{E'E}}{A_Xk_BT}, \tag{2}$$

and of the energy transfer $\varepsilon = \hbar\omega$:

$$\beta = -\frac{\hbar\omega}{k_BT} = -\frac{E - E'}{k_BT}, \tag{3}$$

where $\mu = \cos(\theta)$ is the cosine of the scattering angle in the laboratory system and A_X is the ratio of the mass M_X of the scattering atom X to the neutron mass. An analytical form of $S^T_X(\alpha,\beta)$ was established for a cubic symmetry by using an isotropic harmonic potential which simplifies the complex averaging over all the possible orientations of the molecules. This approximation, known as the Gaussian approximation [10], lead to the following phonon expension:

$$S^T_X(\alpha,\beta) = \mathrm{e}^{-\alpha\lambda_s}\sum_{n=0}^{\infty}\frac{1}{n!}(\alpha\lambda_s)^n\,\mathcal{T}_n(\beta), \tag{4}$$

where λ_s stands for the Debye-Waller coefficient and $\mathcal{T}_n(\beta)$ has the generic form:

$$\mathcal{T}_n(\beta) = \int_{-\infty}^{\infty}\mathcal{T}_1(\beta')\mathcal{T}_{n-1}(\beta-\beta')d\beta'. \tag{5}$$

*e-mail: gilles.noguere@cea.fr

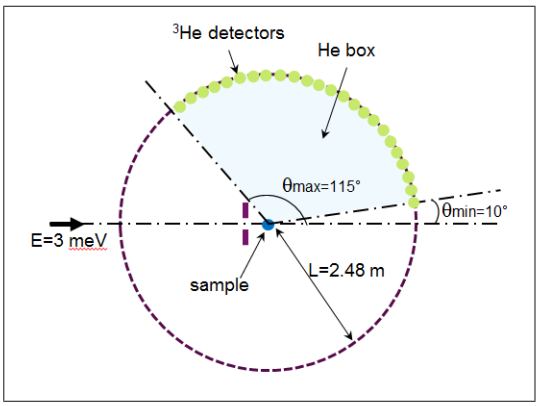

Figure 1. (Color online) Simplified top view of the IN6 time-of-flight spectrometer of the Intitute Laue-Langevin (ILL).

The zero-phonon term $\mathcal{T}_0(\beta) = \delta(\beta)$ corresponds to the elastic peak and the one-phonon term explicitly depends on the phonon density of states $\rho_X^T(\beta)$:

$$\mathcal{T}_1(\beta) = \frac{\rho_X^T(\beta)\mathrm{e}^{-\beta/2}}{2\lambda_s\beta\sinh(\beta/2)}. \quad (6)$$

In the present work, we use *ab intio* phonon spectra obtained at the North Caroline South University from first-principle calculations performed with the VASP code [11].

3 Experiment

Experimental phonon densities of states of UO_2 were deduced from double-differential neutron scattering experiments performed at the IN6 time-of-flight spectrometer of the Intitute Laue-Langevin (ILL). Three temperatures T were investigated, which correspond to "cold" zero-power (300 K), hot-zero power (600 K) and hot-full power (900 K) operating conditions in critical assemblies and pressurized water reactors. A simplified model of IN6 is shown in Fig. 1. The neutron time-of-flight technique consists of measuring the time t traveled by neutrons from the sample until their detection at a given scattering angle θ. The non-relativistic time-energy relation $E' = (72.298L/t)^2$, where E' is in eV, L in meter and t in microseconds, is used to obtain the experimental neutron yield $Y_{exp}^T(\theta, E')$ as a function of the outgoing neutron energies E'. In the present experiment, a rectangular monoenergetic neutron beam of $E = 3$ meV ($\lambda = 5.1$ Å) was focused to the sample, which is mounted in a high temperature furnace placed at the center of the spectrometer. The detection set-up is at a flight distance $L = 2.48(1)$ m from the sample. It forms a ^{3}He detector array that covers scattering angles ranging from 10° to 115°.

The sample is a 4.09(1) cm long cylinder composed of a stack of four depleted UOX pellets of 8.26(1) mm diameter. The total weight of the sample is 23.642(1) g, with a mass-fraction composition in ^{238}U, ^{236}U, ^{235}U, ^{234}U and ^{16}O of 87.598(1)%, 0.005(1)% 0.264(1)% 0.002(1)% and 12.131(1)%, respectively. The UO_2 sample was sealed in a glass tube under vaccum and encapsulated in a niobium sample-holder tube. An empty "dummy" sample was prepared to measure the background contribution.

The experiment consisted in a five days sequence of UO_2 and "dummy" sample measurements, including a short irradiation of a vanadium sample. As this material nearly behaves as a pure incoherent elastic scatterer, its elastic scatering peak is used as reference for calibration purpose and detector efficiency correction. The data reduction steps were handled with the ILL in-house code LAMP.

4 Thermal scattering law

The experimental quantity of interest for this work is the symmetric form of the thermal scattering law $S_{exp}^T(\theta, E')$, from which the contribution of the quasielastic neutron scattering peak is removed. Working in the incoherent scattering approximation leads to:

$$S_{exp}^T(\theta, E') = Y_{exp}^T(\theta, E')\sqrt{\frac{E}{E'}}\mathrm{e}^{\beta/2} - S_{exp_0}^T(\theta, E'). \quad (7)$$

The contribution $S_{exp_0}^T(\theta, E')$ was approximated by a pseudo-Voigt function.

The flight time of each neutron has been simulated with TRIPOLI4®. For convenience, we have only taken into account a central detector ring of 30 cm high, because ^{3}He detectors placed below and above the central detector ring only serve to gain in statistics. The time distribution of the initial neutron burst originating from a Fermi chopper is not included in the simulation. Therefore, $S_{th}^T(\theta, E')$ is calculated from the neutron yields Y_{th}^T provided by TRIPOLI4® as follows:

$$\begin{aligned} S_{th}^T(\theta, E') &= \int_0^{+\infty} R_{E'}(\theta, t) Y_{th}^T(\theta, t)\sqrt{\tfrac{E}{E'}}\mathrm{e}^{\beta/2}\mathrm{d}t \\ &- S_{th_0}^T(\theta, E'). \end{aligned} \quad (8)$$

The probability density functions $R_{E'}(\theta, t)$ stand for the time-dependent experimental response function of the spectrometer. For IN6, the response function is well approximated by a Gaussian. Its full width at half maximum $\Delta t = 43(5)\ \mu s$ was fitted to the elastic peak of the vanadium spectra.

Figure 2 compares the experimental S_{exp}^T and theoretical S_{th}^T obtained at $\theta = 90°$ as a function of the energy transfer ε. The five normal modes of vibration of UO_2 [5] can be distinghuished arround 10 meV, 20 meV, 35 meV, 55 meV and 70 meV. The two first peaks correspond to the translational and longitudinal acoustic modes of the uranium atoms, while the higher energy structures are dominated by the optical modes of the oxygen atoms. At the backward scattering angles, these structures are well reproduced by the simulation. At the forward angles, they are smoothen in the experimental S_{exp}^T due to the multiple scattering of neutrons which have to cross the sample before being detected.

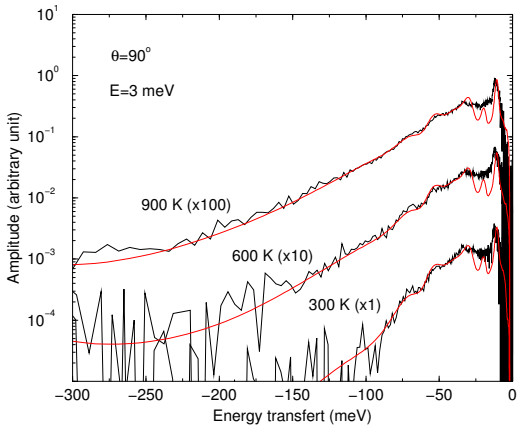

Figure 2. (Color online) Experimental S^T_{exp} and simulated S^T_{th} as a function of the energy transfer $\varepsilon = E - E'$ at 300 K, 600 K and 900 K for $E = 3$ meV and $\theta = 90°$.

5 Phonon density of states

In order to reduce the contribution of the multiple scattering corrections, we decided to determine experimental phonon spectra $\rho^T_{exp}(\beta)$ for UO_2 from neutron yields corresponding to scattering angles ranging from 90° to 115°. By introducing Eq. (6) in Eq. (4) for $n = 1$ and by removing the contribution of the elastic peak ($n = 0$), the incoherent one-phonon approximation leads to:

$$P^T_{exp}(\alpha,\beta) \simeq \frac{2\beta \sinh \beta/2}{\alpha} S^T_{exp}(\alpha,\beta). \quad (9)$$

As finite α boundaries are delimited by the allowed kinematic range of the IN6 spectrometer, $\rho^T_{exp}(\beta)$ can be deduced as follows:

$$\rho^T_{exp}(\beta) \simeq \lim_{\alpha \to 0} P^T_{exp}(\alpha,\beta). \quad (10)$$

In view of obtaining $P^T_{exp}(\alpha,\beta)$ at $\alpha = 0$, we have smooth out fluctuations due to nuclei dynamics by using a log-log extrapolation of the cumulative distribution function of $P^T_{exp}(\alpha,\beta)$. The obtained ρ^T_{exp} are shown in Fig. 3 as a function of the energy transfer ε and are compared to results which have been linearly interpolated between PDOS measured by Pang at 295 K and 1200 K [7]. A satisfactory agreement between the two data sets is observed, at least up to $\varepsilon \simeq 60$ meV. Above 60 meV, the sharp differences come from the increasing broadening of the phonon linewidth due to the response function of IN6, while Pang has concatenated PDOS obtained at three adequately chosen neutron wave lengths, corresponding to incident neutron energies E of 30 meV, 60 meV and 120 meV.

Experimental phonon densities of states of UO_2 can only be compared with their theoretical analogues via TRIPOLI4® simulations that take into account multiphonon and multiple scattering contributions. Figure 4 shows the agreement achieved when the *ab initio* densities of sates established at the North Caroline South University are introduced in the calculations. A closer inspection of the results indicates that the Monte-Carlo simulations are still not able to accurately describe the phonon linewidth broadening, especially arround 30 meV. Similar discrepencies were already pointed out by Pang and are attributed to anharmonic vibrations of the atoms. Indeed, anaharmonicity is always present in real crystal. It may cause interactions among phonons which are neglected in the present model. Despite anharmonic effects in neutron scattering by crystalline materials were the subject of numerical calculations from the early 1960s [13, 14], they still remain an issue to study the resonance line shape of ^{238}U in UO_2 from room temperature to 1800 K [15], or to explain properties of UO_2 in extreme temperature and pressure conditions [16].

6 Conclusions

The present work reports experimental phonon density of states of UO_2 at 300 K, 600 K and 900 K. The comparison of the data with Monte-Carlo simulations confirms that the phonon broadening related to the uranium and oxygen atoms could have different origins. A more sophisticated treatement not only relying on anharmonicity is needed to account for the temperature on interactomic interactions. Following the conclusion of Ref. [21] for actinides, harmonic softening arising from a temperature-dependent harmonic potential could also play a role in the observed results.

References

[1] B.T.M. Willis, Neutron diffraction studies of the actinides oxides I: uranium dioxide and thorium dioxide at room temperature, Proc. R. Soc. London A **274**, 122 (1963).
[2] B.T.M. Willis, Neutron diffraction studies of the actinides oxides II: uranium dioxide and thorium dioxide between room temperature and 1100°C, Proc. R. Soc. London A **274**, 134 (1963).
[3] I.M. Thorson and B.C. Haywood, Scattering law for UO_2, in Proc. of a symposium on inelastic scattering of neutrons in solids and liquids, IAEA report STI/PUB/62, vol. 2, 213, 1963.
[4] Purohit et al.,Inelastic neutron scattering in metal hydrides, UC and UO_2, and applications of the scattering law, in Proc. of a symposium on neutron thermalization and reactor spectra, IAEA report STI/PUB/160, vol. 1, 407, 1967.
[5] G. Dolling, R.A. Cowley and A.D. Woods, Can. J. Phys. **43**, 1397 (1965).
[6] J.W.L. Pang et al., Phys. Rev. Lett. **110**, 157401 (2013).
[7] J.W.L. Pang et al., Phys. Rev. B **89**, 115132 (2014).
[8] L. Van Hove, Phys. Rev. **95**, 249 (1954).
[9] A.W. Solbrig, Am. J. Phys. **29**, 257 (1961).
[10] G. Paym, Phys. Rev. **121**, 741 (1961).
[11] J.L. Wormald and A.I. Hawari, Ab Initio Generation of Thermal Scattering Law for Uranium Dioxide, Trans. American Nucl. Soc. **115** (2016).

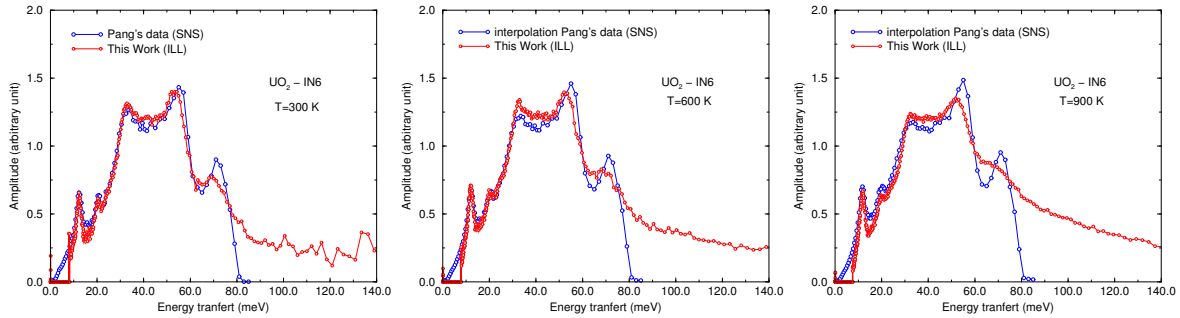

Figure 3. (Color online) Experimental PDOS for UO_2 at 300 K, 600 K and 900 K measured at ILL and SNS [7].

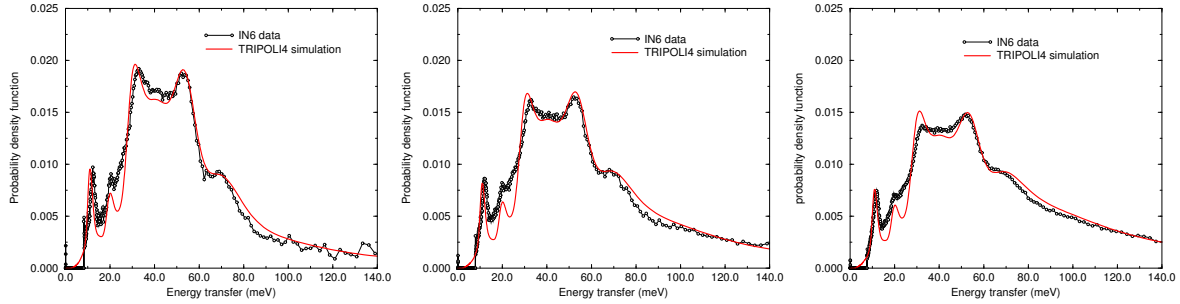

Figure 4. (Color online) Experimental and theoretical PDOS for UO_2 at 300 K, 600 K and 900 K.

[12] E. Brun et al., Ann. Nucl. Ener. **82**, 151 (2015).
[13] A.A. Maradudin and A.E. Fein, Phys. Rev. **128**, 2589 (1962).
[14] J.J.J. Kokkedee, Physica 28, 374 (1962).
[15] R.L. D'Avila and R.A. Karam, Ann. Nucl. Ener. **18**, 249 (1991).
[16] H. Zhang et al., Superionic UO_2: a model anharmonic crystalline material, arXiv:1902.02858, 2019.
[17] R.E. MacFarlane et al., Nucl. Data Sheets **111**, 2739 (2010).
[18] R.E. MacFarlane, New thermal neutron scattering files for ENDF/B-VI, Los Alamos National Laboratory Report LA-12639-MS, 1994.
[19] P. Archier et al., Nucl. Data Sheets **118**, 488 (2014).
[20] Y. Yun, D. Legut and P.M. Oppeneer, J. Nucl. Mater **426**, 109 (2012).
[21] M.E. Manley et al., Phys. Rev. Lett. **86**, 3076 (2001).